INTERNATIONAL JOURNAL FOR NUMERICAL METHODS IN FLUIDS
Int. J. Numer. Meth. Fluids 2009; **60**:791–808
Published online 16 September 2008 in Wiley InterScience (www.interscience.wiley.com). DOI: 10.1002/fld.1919

On the simulation of a time-dependent cavity flow of an Oldroyd-B fluid

Tsorng-Whay Pan*, †, Jian Hao and Roland Glowinski

Department of Mathematics, University of Houston, Houston, TX 77204, U.S.A.

SUMMARY

In this article we present a finite element method for simulating the time-dependent flow of an Oldroyd-B fluid in a lid-driven cavity, which is a stringent test problem at high Weissenberg number. The key considerations for developing the methodology are the preservation of the positive definiteness of the conformation tensor via the log-conformation representation and additional diffusion, from second-order upwind scheme, to smooth the high-frequency modes. The combination of the log-conformation representation, finite element method, and an operator-splitting Lie's scheme, gives us a robust and easy-to-implement scheme. We have obtained convergent results when simulating time-dependent cavity flows.

Received 22 April 2008; Revised 6 August 2008; Accepted 8 August 2008

KEY WORDS: log conformation; Oldroyd-B fluid; Stokes flow; lid-driven cavity; finite element; operator splitting; wave-like equation method

1. INTRODUCTION

Generally, viscoelastic computation in complex flows at high Weissenberg number has proven to be a tremendous challenge, in particular, for systems where singularities are present. Examples include cavity flows with a steadily moving lid, and only a limited number of computational methods provide satisfactory results [1]. There have been few numerical studies of cavity flows of viscoelastic fluids. Phelan *et al.* [2] implemented a hyperbolic numerical solution method and tested their method by considering the cavity flow of a shearing–thinning fluid. Grillet and Shaqfeh [3] used a perturbation technique to investigate the first effects of elasticity on the flow geometry of

*Correspondence to: Tsorng-Whay Pan, Department of Mathematics, University of Houston, Houston, TX 77204, U.S.A.
†E-mail: pan@math.uh.edu

Contract/grant sponsor: NSF; contract/grant numbers: ECS-9527123, CTS-9873236, DMS-9973318, CCR-9902035, DMS-0209066, DMS-0443826

the semi-cavity flow problem. Grillet *et al.* [4] studied the numerical modeling of two-dimensional steady lid-driven cavity flow. They introduced leakage to relieve the corner singularity in the simulations by including small rounded channels at the corners where the fluid can leak through and used a mixed finite element with SUPG (streamline upwind/Petrov–Galerkin) stabilization in the discretization of the constitutive equation for the conformation tensor. In [5], Fattal and Kupferman used a second-order finite difference scheme to simulate the Stokes flow of an Oldroyd-B fluid in a lid-driven cavity. They reformulated the constitutive equation as an equation for the matrix logarithm of the conformation tensor to preserve the property of the positive definiteness of the conformation tensor, which was developed in their earlier work [6]. To discretize the advection term in the constitutive equation, they have applied the Kurganov–Tadmor scheme [7] with min-mod limiter (see e.g. [8] for an extensive reference on limiters). They have pointed out that a numerical instability that arises from the balance between advection and stretching when solving the constitutive equation and the log-conformation technique is a better approach.

From the previous work, we have found that there are two important considerations when trying to simulate time-dependent viscoelastic flows at high Weissenberg number. First, the positive definiteness of the conformation tensor has to be preserved at the *discrete level* during the *entire time integration*. Besides the technique developed in [5], another attempt for obtaining a positive definiteness preserving scheme when discretizing the constitutive equation is a recent work by Lozinski and Owen [9]. They factorize the conformation tensor to get $\mathbf{c} = AA^{\mathrm{T}}$ and then try to write down the equations for A approximately at the discrete level. Hence, the positive definiteness of the conformation tensor is forced with such an approach. In a most recent work [10], Lee and Xu have developed a unified numerical discretization framework that can be used for simulating most of the existing constitutive equations in a way that the positiveness of the conformation tensor of the continuous level can be extended to its discrete analogue. However, the main advantage of using the log-conformation tensor is that we can better resolve the exponential behavior of the conformation tensor in the region where there are boundary layers. In this article we have incorporated the log-conformation tensor technique developed in [5] with an operator-splitting technique to preserve the positive definiteness of the conformation tensor. Second, the constitutive equation is a hyperbolic equation and lacks a diffusion term. In [11], an additional diffusion term added to the constitutive equation for the Oldroyd-B fluid did stabilize the computations. SUPG methods have been used widely with finite element methods (see [1] and the references therein for details) to stabilize the numerical schemes used for solving the constitutive equation. The min-mod limiter used in [5] is known to be very stable but introduces additional diffusion; indeed the additional diffusion obtained directly or indirectly from the above numerical techniques does stabilize to some extent the numerical schemes used for solving the constitutive equation. It is the opinion of the authors that additional (but not too much) diffusion smoothes out some of the high-frequency modes from the discrete conformation tensor so that the numerical scheme is stabilized. To reduce the number of high-frequency modes in the first place, we have chosen a finite element approach for discretizing the conformation tensor defined on a coarser mesh (compared with the mesh for the velocity field); actually in, e.g. [4, 5, 12], the discrete conformation tensor was also defined on coarser meshes.

In [13, 14] the technique of log-conformation tensor has been used with finite element methods to simulate viscoelastic fluid flows past a cylinder. This article is a follow-up of reference [15] in which the points mentioned above had been taken into account to develop a stable scheme for the solution of a two-dimensional lid-driven cavity Stokes flow for an Oldroyd-B fluid at high Weissenberg numbers. In [15] the advection was treated with the first-order upwind scheme which,

DOI: 10.1002/fld

just like the min-mod limiter used in [5], produces too much artificial diffusion. Even though the lid-driven cavity flow has closed planar streamlines in a simple confined geometry, its conformation tensor does have sharp boundary layers attached to the lid at high Weissenberg numbers. The numerical results in [5] and [15] were obtained with uniform meshes and hence, the boundary layer has not been well resolved. In both [5, 15], some convergent results have been shown but the ones such as the convergence of the conformation tensor on the lid have not been shown. In this article we have improved the methodology developed in [15] by applying a second-order upwind to treat the advection and using non-uniform meshes with very fine mesh close to the lid and to the left and right sides of the cavity. With these modifications, we have obtained convergent numerical results for Weissenberg number up to 1. For higher Weissenberg number cases, it is very difficult to resolve the boundary layer of the conformation tensor since its maximum value has shown an exponential relation to the Weissenberg number as discussed in Section 4 unless we use extremely fine meshes close to the lid. In the following section, we first introduce the formulation of the problem. Then we discuss how to apply Lie's scheme to split the constitutive equation into subproblems and how to reformulate those subproblems via the technique developed in [5]. In Section 3, we discuss the space and time discretizations together with numerical methods for solving the subproblems. Numerical results are presented in Section 4.

2. FORMULATION OF THE PROBLEM

We consider a two-dimensional lid-driven cavity Stokes flow for an Oldroyd-B fluid. Let $\Omega=(0,1)\times(0,1)$ be the region occupied by the fluid, Γ the boundary of Ω and $T>0$ (see Figure 1). The flow model problem is governed by

$$-\nabla p+v_s\Delta\mathbf{u}+\frac{v_p}{\lambda_1}\nabla\cdot\mathbf{c}=\mathbf{0}\quad\text{in }\Omega\times(0,T) \tag{1}$$

$$\nabla\cdot\mathbf{u}=0\quad\text{in }\Omega\times(0,T) \tag{2}$$

$$\frac{\partial\mathbf{c}}{\partial t}+(\mathbf{u}\cdot\nabla)\mathbf{c}-(\nabla\mathbf{u})\mathbf{c}-\mathbf{c}(\nabla\mathbf{u})^{\mathrm{T}}=\frac{1}{\lambda_1}(\mathbf{I}-\mathbf{c})\quad\text{in }\Omega\times(0,T) \tag{3}$$

$$\mathbf{c}(0)=\mathbf{c}_0\quad\text{in }\Omega \tag{4}$$

$$\mathbf{u}=\mathbf{g}(t)\quad\text{on }\Gamma\times(0,T)\text{ with }\int_\Gamma\mathbf{g}(t)\cdot\mathbf{n}\,\mathrm{d}\Gamma=0\quad\text{on }(0,T) \tag{5}$$

Here $\mathbf{u}$ and p are the flow velocity and pressure, $\mathbf{c}$ is the conformation tensor, v_s and v_p are the solvent and polymer viscosities, λ_1 is a characteristic relaxation time for the fluid, while $\mathbf{n}$ is the unit outward normal vector at the boundary Γ. We use the notation $v(t)$ to denote the function $\mathbf{x}\to v(\mathbf{x},t)$ in (4), (5) and below.

For $\mathbf{g}(t)$ in (5), we have chosen the same regularized boundary condition given in [5]:

$$\mathbf{g}(\mathbf{x},t)=\begin{cases}(g(x,t),0)^{\mathrm{T}} & \text{on }\{\mathbf{x}|\mathbf{x}=(x,1)^{\mathrm{T}},0<x<1\}\\ (0,0)^{\mathrm{T}} & \text{otherwise on }\Gamma\end{cases} \tag{6}$$

with $g(x,t)=8(1+\tanh 8(t-0.5))x^2(1-x)^2$. The discontinuity of the velocity field at the two upper corners has been removed in (6). The inflow boundary conditions for the conformation

DOI: 10.1002/fld

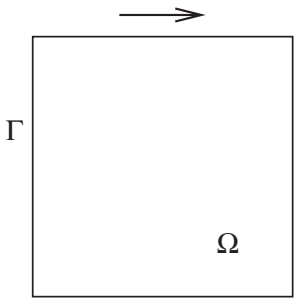

Figure 1. Lid-driven flow in a square cavity.

tensor $\mathbf{c}$ is not needed since there is no inflow boundary for this case. The Weissenberg number is $Wi=\lambda_1 U/L$ where U and L are the characteristic velocity and length scale. With $U=1$ as the speed from the lid and $L=1$ as the width of the cavity, $Wi=\lambda_1$.

We have applied an operator-splitting technique, namely, Lie's scheme [16], to solve (1)–(5). Lie's scheme is *first-order* accurate, but its low-order accuracy is compensated by easy implementation, less cost in computational time, good stability, and robustness properties. For example, it has been successfully applied to develop numerical methods for simulating the interaction of solid particles and fluid (see, e.g. [17–19]). Let Δt be a time discretization step and $t^n=n\Delta t$. Applying the operator-splitting technique to (1)–(5) yields:

For $n\geqslant 0$, $\mathbf{c}^n$ being known, we compute first $\mathbf{u}^{n+1}(\approx\mathbf{u}(t^{n+1}))$ and $p^{n+1}(\approx p(t^{n+1}))$ via the solution of the following problem:

$$-\nabla p^{n+1}+v_s\Delta\mathbf{u}^{n+1}=-\frac{v_p}{\lambda_1}\nabla\cdot\mathbf{c}^n \quad \text{in } \Omega \tag{7}$$

$$\nabla\cdot\mathbf{u}^{n+1}=0 \quad \text{in } \Omega \tag{8}$$

$$\mathbf{u}^{n+1}=\mathbf{g}(t^{n+1}) \quad \text{on } \Gamma \tag{9}$$

Next, we compute $\mathbf{c}^{n+1}$ via the following steps: first solve

$$\frac{\partial\mathbf{c}}{\partial t}+(\mathbf{u}^{n+1}\cdot\nabla)\mathbf{c}=\mathbf{0} \quad \text{in } \Omega\times(t^n,t^{n+1}) \tag{10}$$

$$\mathbf{c}(t^n)=\mathbf{c}^n \quad \text{in } \Omega \tag{11}$$

and set $\mathbf{c}^{n+1/2}=\mathbf{c}(t^{n+1})$. Then solve

$$\frac{\partial\mathbf{c}}{\partial t}-(\nabla\mathbf{u}^{n+1})\mathbf{c}-\mathbf{c}(\nabla\mathbf{u}^{n+1})^{\mathrm{T}}+\frac{1}{\lambda_1}\mathbf{c}=\frac{1}{\lambda_1}\mathbf{I} \quad \text{in } \Omega\times(t^n,t^{n+1}) \tag{12}$$

$$\mathbf{c}(t^n)=\mathbf{c}^{n+1/2} \quad \text{in } \Omega \tag{13}$$

and set $\mathbf{c}^{n+1}=\mathbf{c}(t^{n+1})$.

To keep $\mathbf{c}$ positive definite, we have combined in the following the matrix logarithm of the conformation tensor developed in [5, 6] with the above operator-splitting scheme. But first, for a symmetric positive definite matrix $\mathbf{c}$, we have that $\boldsymbol{\psi}=\log\mathbf{c}$. (Recall that a symmetric positive

DOI: 10.1002/fld

definite matrix A can always be diagonalized as $A = R\Lambda R^{\mathrm{T}}$, and that $\log A = R \log \Lambda R^{\mathrm{T}}$.) In [6], it was shown that with $\mathbf{u}^n$ being a divergence-free velocity field and $\mathbf{c}$ a symmetric positive definite tensor field, the velocity gradient $\nabla \mathbf{u}^n$ can be decomposed as

$$\nabla \mathbf{u}^n = \boldsymbol{\omega}_n + B_n + N_n \mathbf{c}^{-1} \tag{14}$$

where $\boldsymbol{\omega}_n$ and N_n are skew-symmetric, and B_n is symmetric, trace free, and commutes with $\mathbf{c}$. Using these matrices, we obtain the following variant of scheme (7)–(13):

For $n \geqslant 0$, $\mathbf{c}^n$ (and $\boldsymbol{\psi}^n = \log \mathbf{c}^n$) being known, we compute first $\mathbf{u}^{n+1}$ and p^{n+1} via the solution of the following problem:

$$-\nabla p^{n+1} + \nu_{\mathrm{s}} \Delta \mathbf{u}^{n+1} = -\frac{\nu_{\mathrm{p}}}{\lambda_1} \nabla \cdot \mathbf{c}^n \quad \text{in } \Omega \tag{15}$$

$$\nabla \cdot \mathbf{u}^{n+1} = 0 \quad \text{in } \Omega \tag{16}$$

$$\mathbf{u}^{n+1} = \mathbf{g}(t^{n+1}) \quad \text{on } \Gamma \tag{17}$$

Next, we compute $\boldsymbol{\psi}^{n+1}$ via the following steps: first solve

$$\frac{\partial \boldsymbol{\psi}}{\partial t} + (\mathbf{u}^{n+1} \cdot \nabla)\boldsymbol{\psi} = \mathbf{0} \quad \text{in } \Omega \times (t^n, t^{n+1}) \tag{18}$$

$$\boldsymbol{\psi}(t^n) = \boldsymbol{\psi}^n \quad \text{in } \Omega \tag{19}$$

and set $\boldsymbol{\psi}^{n+1/2} = \boldsymbol{\psi}(t^{n+1})$. Then solve

$$\frac{\partial \boldsymbol{\psi}}{\partial t} - [\boldsymbol{\omega}_{n+1}\boldsymbol{\psi} - \boldsymbol{\psi}\boldsymbol{\omega}_{n+1}] - 2B_{n+1} = \frac{1}{\lambda_1}(\mathrm{e}^{-\boldsymbol{\psi}} - \mathbf{I}) \quad \text{in } \Omega \times (t^n, t^{n+1}) \tag{20}$$

$$\boldsymbol{\psi}(t^n) = \boldsymbol{\psi}^{n+1/2} \quad \text{in } \Omega \tag{21}$$

and set $\boldsymbol{\psi}^{n+1} = \boldsymbol{\psi}(t^{n+1})$ and $\mathbf{c}^{n+1} = \mathrm{e}^{\boldsymbol{\psi}^{n+1}}$.

Remark 1

To compute $\boldsymbol{\omega}$, B, and N from a divergence-free velocity field $\mathbf{u}$ for a two-dimensional case, we can use the following formulas given in [6]: (i) If $\mathbf{c}$ is proportional to the unit tensor then set $B = (\nabla \mathbf{u} + (\nabla \mathbf{u})^{\mathrm{T}})/2$ and $\boldsymbol{\omega} = \mathbf{0}$. (ii) Otherwise, diagonalize $\mathbf{c}$ via

$$\mathbf{c} = R \begin{pmatrix} \lambda_1 & 0 \\ 0 & \lambda_2 \end{pmatrix} R^{\mathrm{T}} \tag{22}$$

and set

$$\begin{pmatrix} m_{11} & m_{12} \\ m_{21} & m_{22} \end{pmatrix} = R^{\mathrm{T}} (\nabla \mathbf{u}) R \tag{23}$$

Then,

$$N = R \begin{pmatrix} 0 & n \\ -n & 0 \end{pmatrix} R^{\mathrm{T}}, \quad B = R \begin{pmatrix} m_{11} & 0 \\ 0 & m_{22} \end{pmatrix} R^{\mathrm{T}}, \quad \boldsymbol{\omega} = R \begin{pmatrix} 0 & s \\ -s & 0 \end{pmatrix} R^{\mathrm{T}} \tag{24}$$

with $n = (m_{12} + m_{21})/(\lambda_1^{-1} - \lambda_2^{-1})$, and $s = (\lambda_2 m_{12} + \lambda_1 m_{21})/(\lambda_2 - \lambda_1)$.

DOI: 10.1002/fld

Remark 2

Subproblem (18) and (19) is an advection problem. To solve it we advocate the wave-like equation method discussed below. The idea of solving advection-dominated problems via the solution of associated wave-like equations is not new; it has been advocated, for example, in [20] for the solution of the shallow water equations and in [21] for the solution of multidimensional transport problems. It was first introduced in [22] (to our knowledge) when the wave-like equation method was combined by an operator-splitting technique to solve the Navier–Stokes equations for incompressible fluid flow. The method has been tested with the classical wall-driven cavity flow for Reynolds number up to 10 000 [23, 24] and the wall-driven flow in a two-dimensional semi-circular cavity with unstructured meshes for Reynolds number up to 8000 [25]. More results can be found in, e.g. [17–19].

Each entry of the matrix $\boldsymbol{\psi}$ in (18) and (19) satisfies a *transport equation* of the following type:

$$\begin{aligned} &\frac{\partial \varphi}{\partial t}+\mathbf{V}\cdot\nabla\varphi=0 \quad \text{in } \Omega\times(t^n,t^{n+1}) \\ &\varphi(t^n)=\varphi_0 \quad \text{in } \Omega \end{aligned} \tag{25}$$

with $\nabla\cdot\mathbf{V}=0$ and $\partial\mathbf{V}/\partial t=\mathbf{0}$ on (t^n,t^{n+1}).

Using the properties $\nabla\cdot\mathbf{V}=0$ and $\partial\mathbf{V}/\partial t=\mathbf{0}$ on $\Omega\times(t^n,t^{n+1})$, we have that problem (25) is 'equivalent' to the (formally) well-posed problem:

$$\begin{aligned} &\frac{\partial^2\varphi}{\partial t^2}-\nabla\cdot((\mathbf{V}\cdot\nabla\varphi)\mathbf{V})=0 \quad \text{in } \Omega\times(t^n,t^{n+1}) \\ &\varphi(t^n)=\varphi_0, \quad \frac{\partial\varphi}{\partial t}(t^n)=-\mathbf{V}\cdot\nabla\varphi_0 \\ &\mathbf{V}\cdot\mathbf{n}\left(\frac{\partial\varphi}{\partial t}+\mathbf{V}\cdot\nabla\varphi\right)=0 \quad \text{on } \Gamma\times(t^n,t^{n+1}) \end{aligned} \tag{26}$$

Solving the *wave-like equation* (26) by a classical finite element/time-stepping method is quite easy since a variational formulation of (26) is given as

$$\begin{aligned} &\int_\Omega \frac{\partial^2\varphi}{\partial t^2}v\,\mathrm{d}\mathbf{x}+\int_\Omega(\mathbf{V}\cdot\nabla\varphi)(\mathbf{V}\cdot\nabla v)\,\mathrm{d}\mathbf{x}=0 \quad \forall v\in H^1(\Omega) \text{ a.e. on } (t^n,t^{n+1}) \\ &\varphi(t^n)=\varphi_0, \quad \frac{\partial\varphi}{\partial t}(t^n)=-\mathbf{V}\cdot\nabla\varphi_0 \end{aligned} \tag{27}$$

since we have $\mathbf{V}\cdot\mathbf{n}=0$. A solution method for problem (27) will be described in the following section.

Remark 3

Actually, subproblem (20) and (21) can be solved directly using a further splitting, namely,

$$\frac{\partial\boldsymbol{\psi}}{\partial t}-[\boldsymbol{\omega}_{n+1}\boldsymbol{\psi}-\boldsymbol{\psi}\boldsymbol{\omega}_{n+1}]-2B_{n+1}=\mathbf{0} \quad \text{in } \Omega\times(t^n,t^{n+1}) \tag{28}$$

$$\boldsymbol{\psi}(t^n)=\boldsymbol{\psi}^{n+1/2} \quad \text{in } \Omega \tag{29}$$

DOI: 10.1002/fld

and set $\tilde{\boldsymbol{\psi}}^{n+1}=\boldsymbol{\psi}(t^{n+1})$ and $\tilde{\mathbf{c}}^{n+1}=\mathrm{e}^{\tilde{\boldsymbol{\psi}}^{n+1}}$. Then solve

$$\frac{\partial \mathbf{c}}{\partial t}=\frac{1}{\lambda_1}(\mathbf{I}-\mathbf{c}) \quad \text{in } \Omega\times(t^n,t^{n+1}) \tag{30}$$

$$\mathbf{c}(t^n)=\tilde{\mathbf{c}}^{n+1} \quad \text{in } \Omega \tag{31}$$

and set $\mathbf{c}^{n+1}=\mathbf{c}(t^{n+1})$ and $\boldsymbol{\psi}^{n+1}=\log(\mathbf{c}^{n+1})$.

The closed-form solutions of the above two subproblems can be obtained easily (at least for two-dimensional flows).

3. SPACE AND TIME DISCRETIZATIONS

Concerning the *space approximation*, we use P_1-iso-P_2 and P_1 finite elements for the velocity field and pressure, respectively (as, e.g. in [26, 27]). More precisely, with h as the *space discretization step* we introduce a finite element triangulation $\mathscr{T}_h$ of $\overline{\Omega}$ and then $\mathscr{T}_{2h}$ a triangulation twice coarser (in practice we should construct $\mathscr{T}_{2h}$ first and then $\mathscr{T}_h$ by joining the midpoints of the edges of $\mathscr{T}_{2h}$, dividing thus each triangle of $\mathscr{T}_{2h}$ into four similar subtriangles, as shown in Figure 2).

Next, we define the following finite-dimensional spaces:

$$V_{\mathbf{g}_h(t)}=\{\mathbf{v}_h|\mathbf{v}_h\in(C^0(\overline{\Omega}))^2,\mathbf{v}_h|_T\in P_1\times P_1\ \forall T\in\mathscr{T}_h,\mathbf{v}_h|_\Gamma=\mathbf{g}_h(t)\} \tag{32}$$

$$V_{0h}=\{\mathbf{v}_h|\mathbf{v}_h\in(C^0(\overline{\Omega}))^2,\mathbf{v}_h|_T\in P_1\times P_1\ \forall T\in\mathscr{T}_h,\mathbf{v}_h|_\Gamma=\mathbf{0}\} \tag{33}$$

$$L^2_h=\{q_h|q_h\in C^0(\overline{\Omega}),q_h|_T\in P_1\ \forall T\in\mathscr{T}_{2h}\} \tag{34}$$

$$L^2_{0h}=\left\{q_h|q_h\in L^2_h,\int_\Omega q_h\,\mathrm{d}\mathbf{x}=0\right\} \tag{35}$$

in (32)–(35), $\mathbf{g}_h(t)$ is an approximation of $\mathbf{g}(t)$ verifying $\int_\Gamma \mathbf{g}_h(t)\cdot\mathbf{n}\,\mathrm{d}\Gamma=0$ and P_1 is the space of the polynomials in two variables of degree $\leqslant 1$. The discrete conformation tensor belongs to

$$\mathbf{W}_2=\left\{A_h|A_h=\begin{pmatrix}A_{1,h} & A_{2,h}\\ A_{2,h} & A_{3,h}\end{pmatrix},\ A_{i,h}\in L^2_h,\ i=1,2,3\right\} \tag{36}$$

Using these finite element spaces, we obtain the following realization of scheme (15)–(21) (after dropping some of the subscripts h):

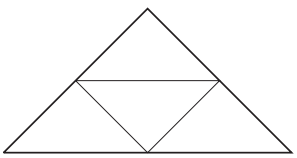

Figure 2. Subdivision of a triangle of $\mathscr{T}_{2h}$.

DOI: 10.1002/fld

For $n \geqslant 0$, $\mathbf{c}^n$ (and $\boldsymbol{\psi}^n$) being known, we compute first $\mathbf{u}^{n+1}$ and p^{n+1} via the solution of the following problem:

$$\begin{gathered}\int_\Omega p^{n+1}\nabla\cdot\mathbf{v}\,d\mathbf{x}-\nu_s\int_\Omega \nabla\mathbf{u}^{n+1}:\mathbf{v}\,d\mathbf{x}=-\frac{\nu_p}{\lambda_1}\int_\Omega(\nabla\cdot\mathbf{c}^n)\cdot\mathbf{v}\,d\mathbf{x}\quad\forall\mathbf{v}\in V_{0h}\\ \int_\Omega q\nabla\cdot\mathbf{u}^{n+1}\,d\mathbf{x}=0\quad\forall q\in L^2_h\\ \mathbf{u}^{n+1}\in V^{n+1}_{\mathbf{g}_h},\quad p^{n+1}\in L^2_{0h}\end{gathered}\tag{37}$$

Next, we compute $\boldsymbol{\psi}^{n+1}=\begin{pmatrix}\psi_1^{n+1} & \psi_2^{n+1}\\ \psi_2^{n+1} & \psi_3^{n+1}\end{pmatrix}$ via the following steps: first solve

$$\begin{gathered}\int_\Omega\frac{\partial^2\psi_i}{\partial t^2}v\,d\mathbf{x}+\int_\Omega(\mathbf{u}^{n+1}\cdot\nabla\psi_i)(\mathbf{u}^{n+1}\cdot\nabla v)\,d\mathbf{x}=0\quad\forall v\in L^2_h\ \text{ on }(t^n,t^{n+1})\\ \psi_i(t^n)=\psi_i^n,\quad\frac{\partial\psi_i}{\partial t}(t^n)=-\mathbf{u}^{n+1}\cdot\nabla\psi_i^n;\quad\psi_i(t)\in L^2_h\end{gathered}\tag{38}$$

for $i=1,2,3$, and set $\boldsymbol{\psi}^{n+1/2}=\begin{pmatrix}\psi_1(t^{n+1}) & \psi_2(t^{n+1})\\ \psi_2(t^{n+1}) & \psi_3(t^{n+1})\end{pmatrix}$. Then solve

$$\begin{aligned}&\int_\Omega\left[\frac{\partial\boldsymbol{\psi}}{\partial t}-(\boldsymbol{\omega}_{n+1}\boldsymbol{\psi}-\boldsymbol{\psi}\boldsymbol{\omega}_{n+1})-2B_{n+1}\right]:\mathbf{T}\,d\mathbf{x}\\ &\quad=\int_\Omega\left[\frac{1}{\lambda_1}(e^{-\boldsymbol{\psi}}-\mathbf{I})\right]:\mathbf{T}\,d\mathbf{x}\quad\forall\mathbf{T}\in\mathbf{W}_2\ \text{ on }(t^n,t^{n+1})\end{aligned}\tag{39}$$

$$\boldsymbol{\psi}(t^n)=\boldsymbol{\psi}^{n+1/2};\quad\boldsymbol{\psi}(t)\in\mathbf{W}_2\tag{40}$$

and set $\boldsymbol{\psi}^{n+1}=\boldsymbol{\psi}(t^{n+1})$ and $\mathbf{c}^{n+1}=e^{\boldsymbol{\psi}^{n+1}}$.

In (37), $V^{n+1}_{\mathbf{g}_h}=V_{\mathbf{g}_h(t^{n+1})}$, and

$$A:B=a_{11}b_{11}+a_{12}b_{12}+a_{21}b_{21}+a_{22}b_{22}\quad\text{for }A=\begin{pmatrix}a_{11} & a_{12}\\ a_{21} & a_{22}\end{pmatrix},\ B=\begin{pmatrix}b_{11} & b_{12}\\ b_{21} & b_{22}\end{pmatrix}$$

At each step in the above scheme, we encounter simpler subproblems that can be solved by *simple and standard* numerical methods. First, the Stokes problem (37) is a classical problem and has been solved by an Uzawa/conjugate gradient algorithm [17], in which a sequence of elliptic problems have been solved by a red–black SOR iterative method. The wave-like equation (38) is solved by the following time-stepping method with its own local sub-timestep:

We first define a sub-timestep, $\tau_1>0$, by $\tau_1=\Delta t/Q_1$, where Q_1 is a positive integer and we time discretize problem (38) by

$$\varphi^0=\varphi_0\tag{41}$$

$$\begin{gathered}\int_\Omega(\varphi^{-1}-\varphi^1)v\,d\mathbf{x}=2\tau_1\int_\Omega(\mathbf{V}\cdot\nabla\varphi^0)v\,d\mathbf{x}\quad\forall v\in L^2_h\\ \varphi^{-1}-\varphi^1\in L^2_h;\quad\varphi^{-1}-\varphi^1=0\quad\text{on }\Gamma\end{gathered}\tag{42}$$

DOI: 10.1002/fld

and for $q=0,\ldots,Q_1-1$,

$$\varphi^{q+1}\in L_h^2$$

$$\int_\Omega \frac{\varphi^{q+1}+\varphi^{q-1}-2\varphi^q}{\tau_1^2}v\,\mathrm{d}\mathbf{x}+\int_\Omega(\mathbf{V}\cdot\nabla\varphi^q)(\mathbf{V}\cdot\nabla v)\,\mathrm{d}\mathbf{x}=0\quad\forall v\in L_h^2 \tag{43}$$

where, in (41) and (43), φ_0 is the initial value and $\mathbf{V}=\mathbf{u}^{n+1}$.

When solving subproblem (39) and (40), we have applied the trapezoidal rule to get a pointwise differential equation at each grid point and then solve it via the further splitting discussed in Remark 3. In (39), $\nabla\mathbf{u}^{n+1}$ is computed via second-order difference scheme on the mesh points used for the conformation tensor and then $\boldsymbol{\omega}_{n+1}$ and B_{n+1} are computed according to (22)–(24).

Remark 4

Scheme (41)–(43) is a centered scheme, which is formally second-order accurate with respect to space and time discretizations. To be stable, scheme (41)–(43) has to verify a condition such as

$$\tau_1\leqslant ch \tag{44}$$

with c of the order of $1/\|\mathbf{V}\|$. Since the advection problem is decoupled from the rest, we can choose the proper time step here so that the above condition is satisfied. Here, we have used the trapezoidal rule to compute the first integral in (43); the above scheme becomes *explicit*, i.e. φ^{q+1} is obtained via the solution of a linear system with a *diagonal* matrix. Another detail is that at each time step in scheme (41)–(43) we do not update the values of φ^q at the boundary grid points not located on the top lid since we have $\mathbf{V}=\mathbf{0}$.

Scheme (41)–(43) has a flavor of the streamline-diffusion methods. For example, when we set $Q_1=1$, (41)–(43) becomes

$$\int_\Omega\frac{\varphi^1-\varphi^0}{\Delta t}v\,\mathrm{d}\mathbf{x}+\int_\Omega(\mathbf{V}\cdot\nabla\varphi^0)v\,\mathrm{d}\mathbf{x}+\frac{\Delta t}{2}\int_\Omega(\mathbf{V}\cdot\nabla\varphi^0)(\mathbf{V}\cdot\nabla v)\,\mathrm{d}\mathbf{x}=0\quad\forall v\in L_h^2;\ \ \varphi^1\in L_h^2 \tag{45}$$

The third term in (45) is a naturally built-in diffusion term only acting in the direction of streamlines.

When computing $\mathbf{V}\cdot\nabla f$ in (42) and (43), the first-order upwind scheme used in [15] produces too much artificial diffusion. We have applied the second-order upwind scheme in this article.

4. NUMERICAL RESULTS

In this section we consider the numerical results for the lid-driven cavity Stokes flow by the numerical schemes described in the above sections. The boundary condition for the velocity field in (6) is given as

$$\mathbf{g}(\mathbf{x},t)=\begin{cases}(g(x,t),0)^{\mathrm{T}} & \text{on } \{\mathbf{x}|\mathbf{x}=(x,1)^{\mathrm{T}},0<x<1\}\\ (0,0)^{\mathrm{T}} & \text{otherwise on } \Gamma\end{cases}$$

DOI: 10.1002/fld

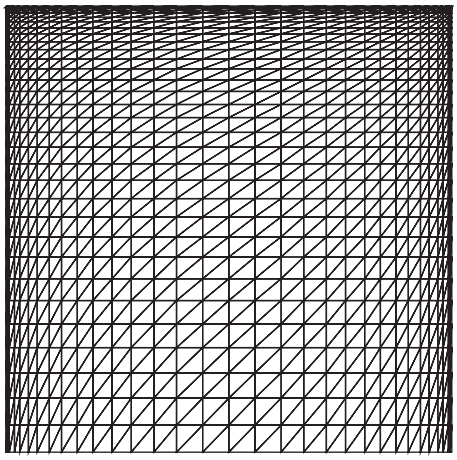

Figure 3. An example of mesh $\mathscr{T}_h$ for $N=32$.

with $g(x,t)=8(1+\tanh 8(t-0.5)x^2(1-x)^2)$; this choice gives a smooth start and for $t\gg\frac{1}{2}$, the lid velocity attains its maximum, $\mathbf{u}=(1,0)^{\mathrm{T}}$, and at the center, $x=1/2$. The initial condition for $\mathbf{c}$ is $\mathbf{c}_0=\mathbf{I}$. Both the viscosities, ν_{s} and ν_{p}, in all calculations are equal to 1. The relaxation times λ_1 considered here are 0.5 and 1 (so the Weissenberg numbers are 0.5 and 1, respectively).

The mesh $\mathscr{T}_{2h}$ for the pressure is a triangular mesh obtained in the following way. We have chosen points $y_j=1-(1-2j/N)^2$, for $j=0,1,\ldots,N/2$, in the y-direction and in the x-direction, we first choose $x_i=2(2i/N)^2$, for $i=0,1,\ldots,N/4$, and then set $x_i=1-x_{N/2-i}$, for $i=N/4+1,\ldots,N/2$. Using lines $x=x_i$ and $y=y_j$, for $i,j=1,\ldots,N/2-1$, we divide the unit square into smaller rectangles and each rectangle is divided into two triangles. After obtaining the triangular mesh for the pressure, we joined the midpoints of the edges of each triangle to divide it into four smaller triangles, as shown in Figure 2, to obtain the mesh for the velocity field. In Figure 3 an example mesh for the velocity field for $N=32$ is shown. With non-uniform triangular meshes, the discrete elliptic problems arising from the Uzawa conjugate gradient algorithm at each iteration have been solved by a red–black SOR iterative method. We have parallelized the code via OpenMP and run it on quad-core CPUs to speed up the computation. To obtain stationary state we need to reach $t=20$ (resp., 30) for $We=0.5$ (resp., $We=1$).

4.1. $Wi=0.5$

This is a 'good' test case since the Weissenberg number is not too high. The results obtained with $N=256$, 288, and 320 are computed with the time steps $\Delta t=0.0015, 0.0012$, and 0.001, respectively. The kinetic energy grows as the lid accelerates, reaches a maximum at the end of the acceleration, and decreases toward a steady value as elastic energy builds up. The history of the kinetic energy, $\frac{1}{2}\|\mathbf{u}_h\|_2^2$, and the history of the elastic energy, $\int_\Omega(c_{11}+c_{22})\,\mathrm{d}\mathbf{x}$, are shown in Figure 5. We have obtained a steady-state solution for $Wi=0.5$ as shown by the kinetic and elastic energy in Figure 5. The streamlines and the density plots of ψ_{ij} obtained with $N=256$ at $t=20$ are shown in Figure 4. The smallest value of the stream function obtained with $N=256$ and $\Delta t=0.0015$ is -0.07000558 at $(0.4692383, 0.7981873)$. The cross sections

DOI: 10.1002/fld

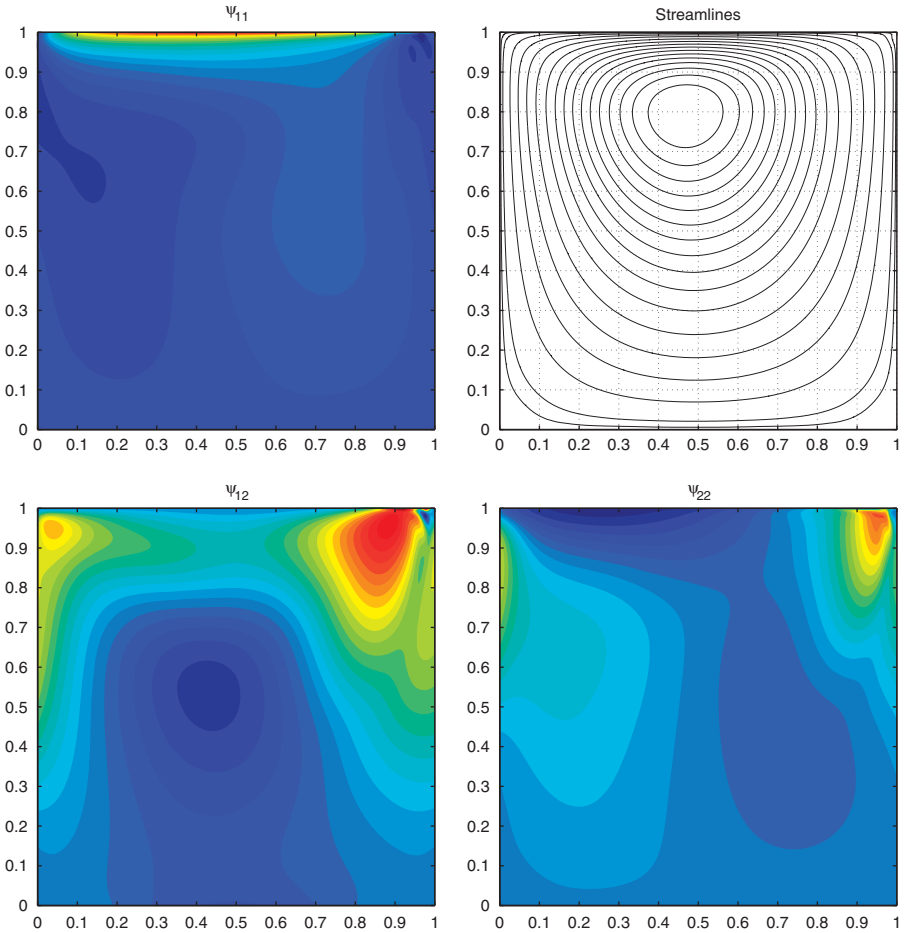

Figure 4. The density plots of ψ_{11} (upper left), ψ_{12} (lower left), ψ_{22} (lower right), and the streamlines (upper right) obtained with $N=256$ at $t=20$ for $Wi=0.5$.

of ψ_{ij} at $x=0.5$ and at $y=1$, c_{ij} at $y=1$ and u_1 at $x=0.5$ and u_2 at $y=0.75$ are shown in Figures 5 and 6. These results show the convergence when reducing the mesh size and time step. As shown in Figures 5 and 6, c_{11} and c_{22} do have sharp boundary layer attached to the lid. The center of the core vortex region shifts in the upstream direction as observed in the experiments [28].

4.2. $Wi=1$

In this section the results obtained with $N=288$, 320, and 352 are computed with the time steps $\Delta t=0.0015, 0.0012$, and 0.001, respectively. The kinetic energy and elastic energy behave like those of the case $Wi=0.5$. Their histories are shown in Figure 7. We have obtained a steady-state solution for $Wi=1$. The smallest value of the stream function obtained with $N=352$ and $\Delta t=0.001$

DOI: 10.1002/fld

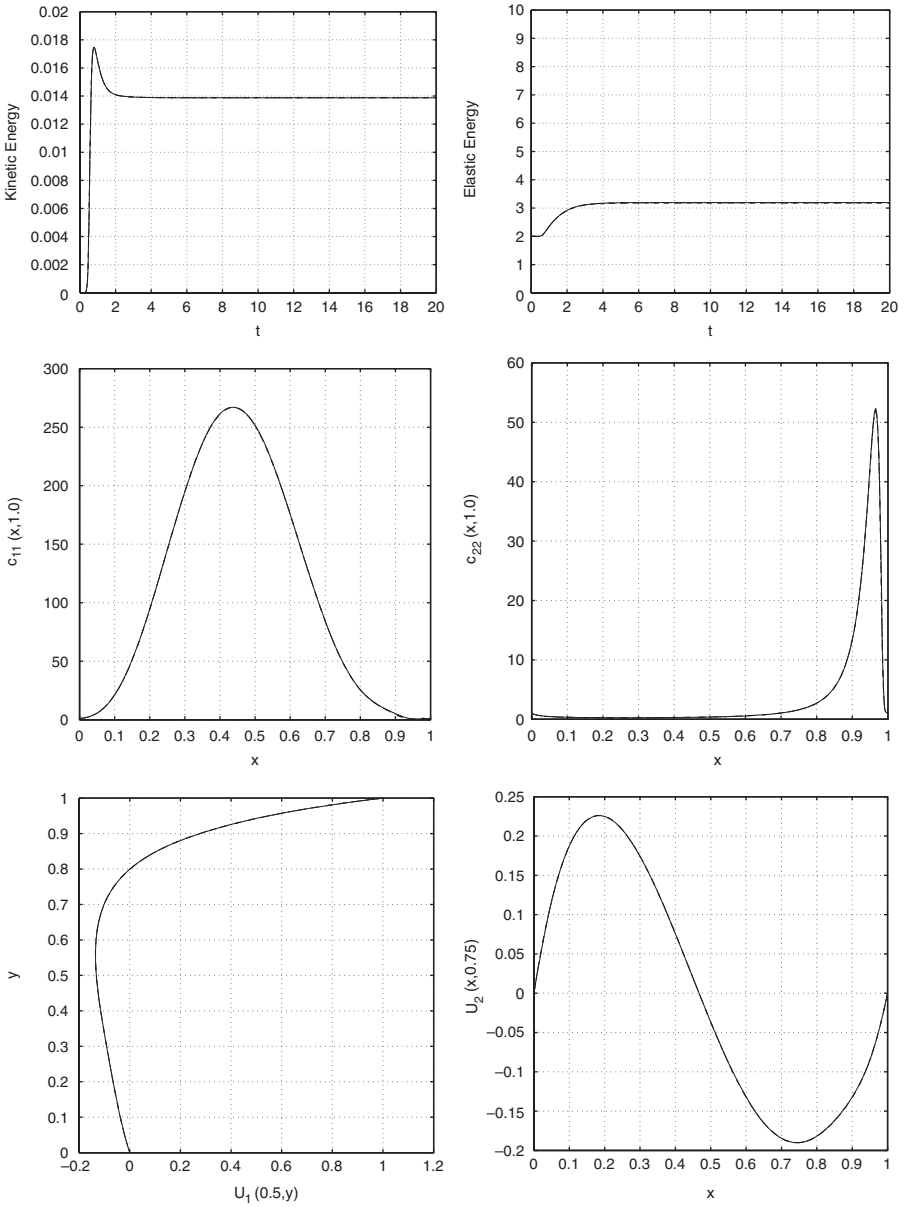

Figure 5. Histories of the kinetic energy (upper left) and the elastic energy (upper right), and the cross section of $c_{11}(x,1)$ (middle left), $c_{22}(x,1)$ (middle right), $u_1(0.5,y)$ (lower left), and $u_2(x,0.75)$ (lower right) at $t=20$ obtained with $N=256$ (dashed line), 288 (dash-dotted line), and 320 (solid line) for $Wi=0.5$.

DOI: 10.1002/fld

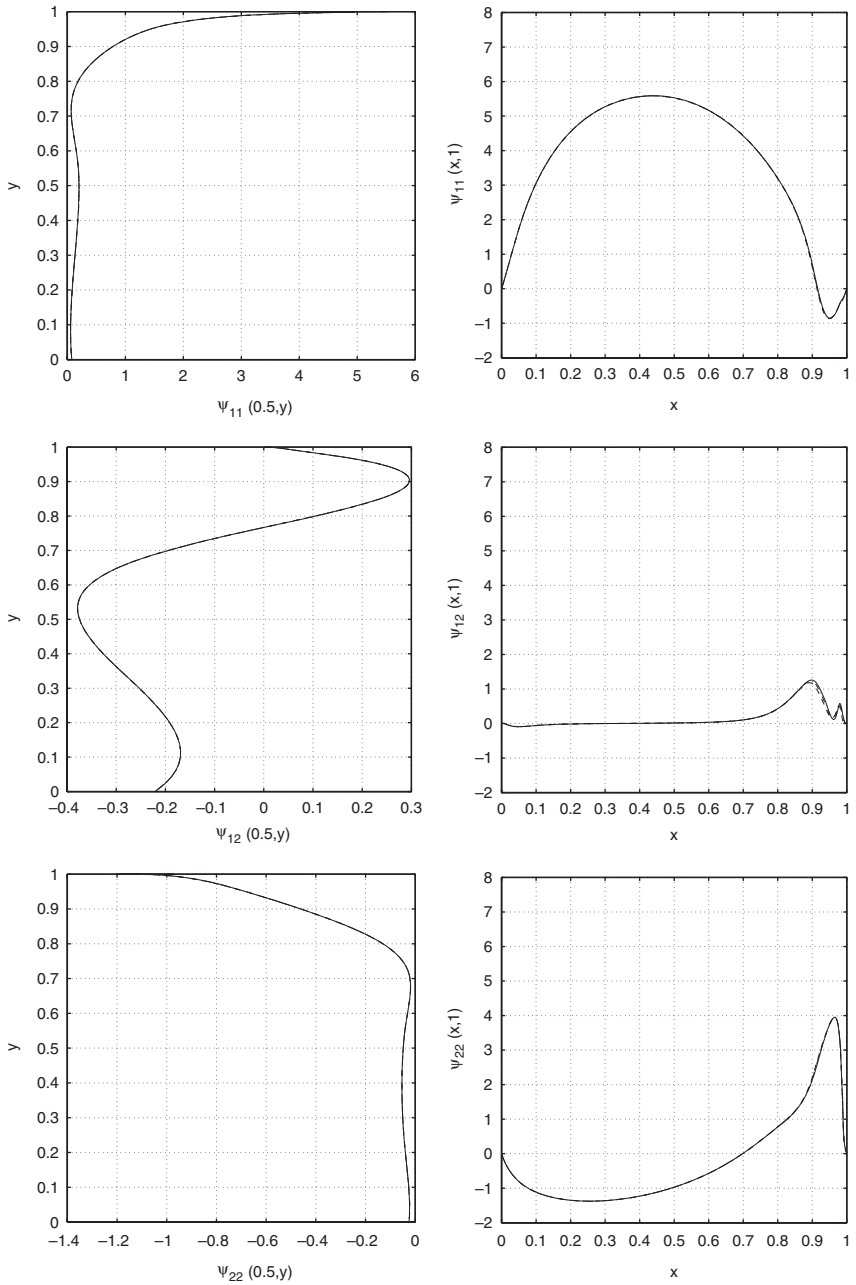

Figure 6. The cross section of ψ_{11}, ψ_{12}, and ψ_{22} (from top to bottom) at $x=0.5$ (left) and $y=1$ (right) obtained with $N=256$ (dashed line), 288 (dash-dotted line), and 320 (solid line) at $t=20$ for $Wi=0.5$.

DOI: 10.1002/fld

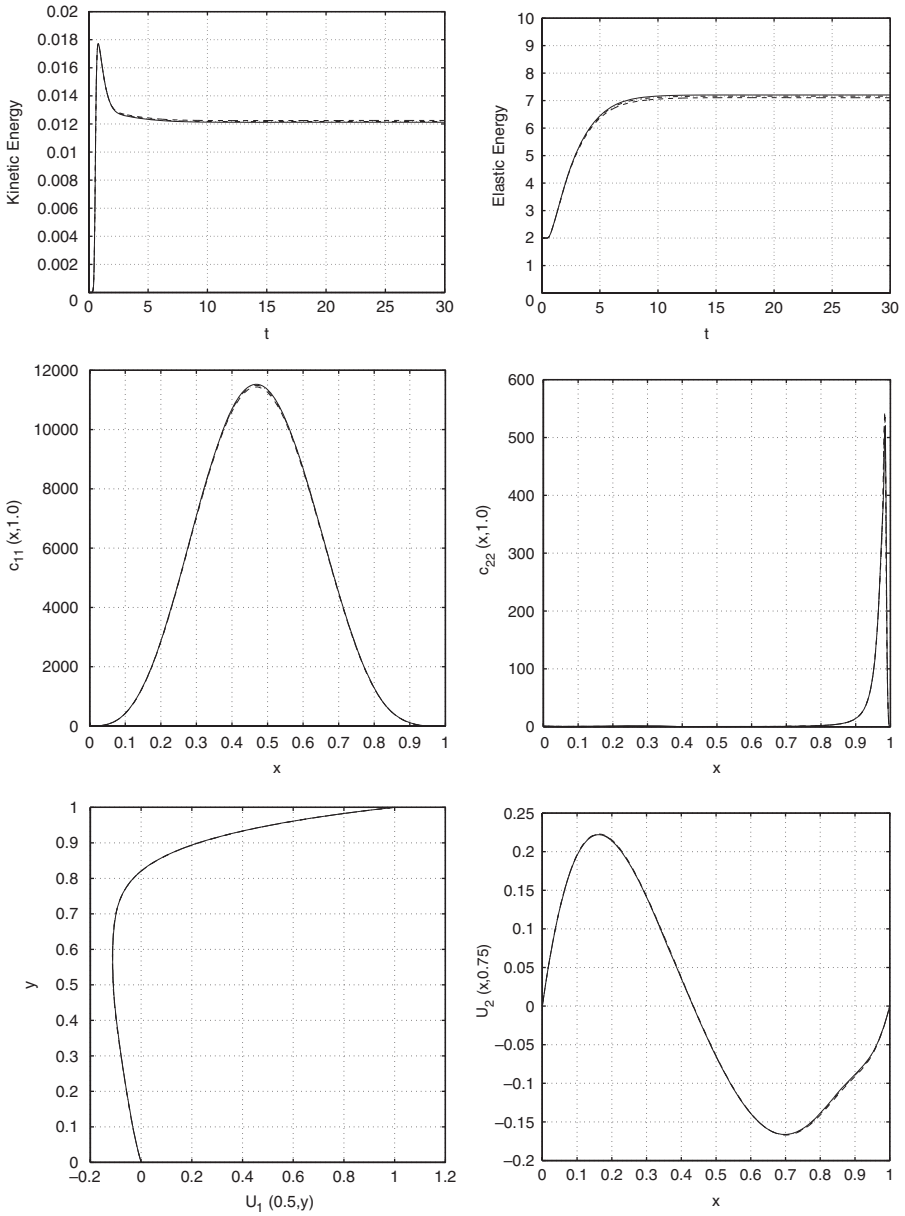

Figure 7. Histories of the kinetic energy (upper left) and the elastic energy (upper right), the cross section of $c_{11}(x,1)$ (middle left), $c_{22}(x,1)$ (middle right), $u_1(0.5,y)$ (lower left), and $u_2(x,0.75)$ (lower right) at $t=30$ obtained with $N=288$ (dashed line), $N=320$ (dash-dotted line), and $N=352$ (solid line) for $Wi=1$.

DOI: 10.1002/fld

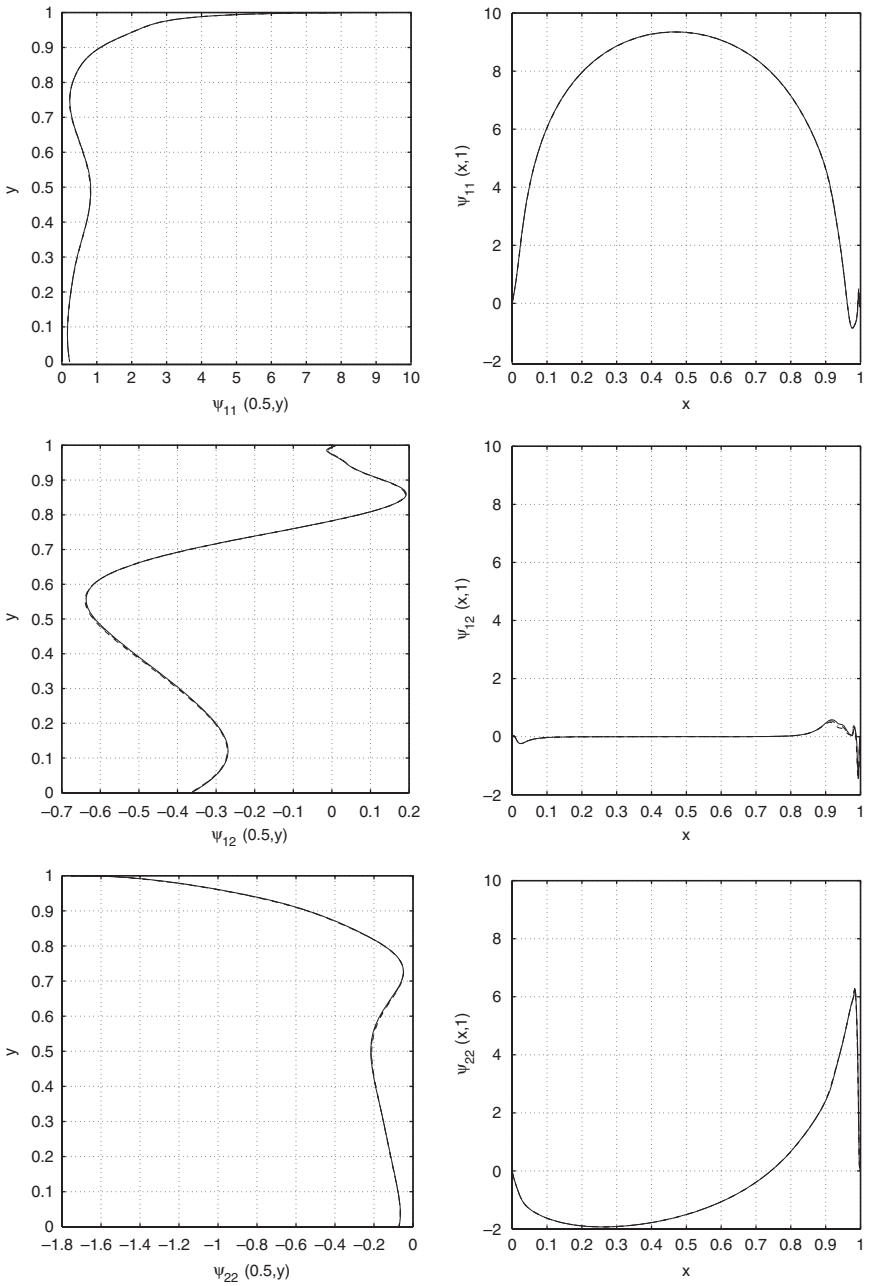

Figure 8. The cross section of ψ_{11}, ψ_{12}, and ψ_{22} (from top to bottom) at $x=0.5$ (left) and $y=1$ (right) obtained with $N=288$ (dashed line), 320 (dash-dotted line), and 352 (solid line) at $t=30$ for $Wi=1$.

DOI: 10.1002/fld

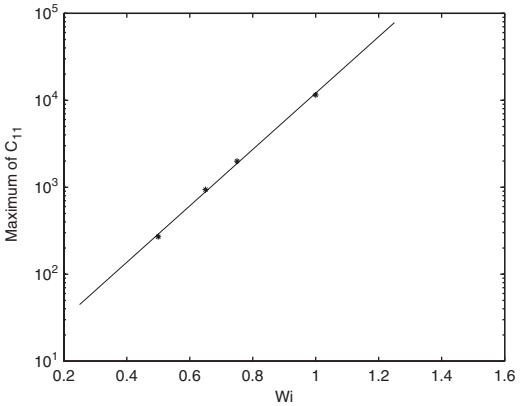

Figure 9. The exponential curve fitting for the maximum of c_{11} and Wi.

is -0.06383407 at $(0.4394693, 0.8159704)$. The cross sections of ψ_{ij} at $x=0.5$ and at $y=1$, c_{11} and c_{22} at $y=1$ and u_1 at $x=0.5$ and u_2 at $y=0.75$ are shown in Figures 7 and 8. These results show the convergence when reducing the mesh size and time step. As shown in Figures 7 and 8, the boundary layer of c_{11} attached to the lid becomes much higher. The maximum of c_{11} is 11 529.43 obtained with $N=352$ at $t=30$.

The largest values of ψ_{11} at $x=0.5$ shown in [5] for $Wi=1$ are less than 7. Our values shown in Figure 8 are about 9.33. We believe that these values obtained in [5] for $Wi=1$ were not well-resolved due to the use of uniform meshes that are not very fine mesh close to the lid. In addition, they might be smoothed out by the numerical diffusion produced by the Kurganov–Tadmor scheme with min-mod limiter used in [5].

4.3. The growth of c_{11}

Using the curve fitting for the maximum of c_{11} obtained at $Wi=0.5, 0.65, 0.75$, and 1, we have obtained the relation $c_{11}(Wi)=e^{1.9346+7.4667Wi}$ and its plot is shown in Figure 9. It gives us a hint that we need very fine meshes to resolve the boundary layer for the cases of Weissenberg number higher than 1.

5. CONCLUSION

We have presented a finite element method for simulating the time-dependent flow of an Oldroyd-B fluid. This method is robust and easy to implement when simulating time-dependent cavity flows at high Weissenberg numbers. The log-conformation representation and the fine mesh next to the lid do help significantly when dealing with the conformation tensor at high Weissenberg number. The numerical treatment of the advection term is also crucial. The method of characteristics could be another choice for solving the advection problem as done in [10, 29] to preserve the positive definiteness of the conformation tensor when using operator-splitting techniques.

DOI: 10.1002/fld

ACKNOWLEDGEMENTS

We acknowledge the helpful comments of E. Dean, D.D. Joseph, A. Lozinski, M. Pasquali and P. Singh and the support of NSF (grants ECS-9527123, CTS-9873236, DMS-9973318, CCR-9902035, DMS-0209066, DMS-0443826).

REFERENCES

1. Baaijens FPT. Mixed finite element methods for viscoelastic flow analysis: a review. *Journal of Non-Newtonian Fluid Mechanics* 1998; **79**:361–385.
2. Phelan FR, Malone MF, Winter HH. A purely hyperbolic model for unsteady viscoelastic flow. *Journal of Non-Newtonian Fluid Mechanics* 1989; **32**:197–224.
3. Grillet AM, Shaqfeh ESG. Observations of viscoelastic instabilities in recirculation flows of Boger fluids. *Journal of Non-Newtonian Fluid Mechanics* 1996; **64**:141–155.
4. Grillet AM, Yang B, Khomami B, Shaqfeh ESG. Modeling of viscoelastic lid driven cavity flow using finite element simulations. *Journal of Non-Newtonian Fluid Mechanics* 1999; **88**:99–131.
5. Fattal R, Kupferman R. Time-dependent simulation of viscoelastic flows at high Weissenberg number using the log-conformation representation. *Journal of Non-Newtonian Fluid Mechanics* 2005; **126**:23–37.
6. Fattal R, Kupferman R. Constitutive laws for the matrix-logarithm of the conformation tensor. *Journal of Non-Newtonian Fluid Mechanics* 2004; **123**:281–285.
7. Kurganov A, Tadmor E. New high-resolution central schemes for nonlinear conservation laws and convection-diffusion equations. *Journal of Computational Physics* 2000; **160**:241–282.
8. LeVeque R. *Numerical Methods for Conservation Laws*. Birkhäuser: Basel, 1992.
9. Lozinski A, Owen RG. An energy estimate for the Oldroyd-B model: theory and applications. *Journal of Non-Newtonian Fluid Mechanics* 2003; **112**:161–176.
10. Lee YJ, Xu J. New formulations, positivity preserving discretizations and stability analysis for non-Newtonian flow models. *Computer Methods in Applied Mechanics and Engineering* 2006; **195**:1180–1206.
11. Sureshkumar R, Beris AN. Effect of artificial stress diffusivity on the stability of numerical calculations and the flow dynamics of time-dependent viscoelastic flows. *Journal of Non-Newtonian Fluid Mechanics* 1995; **60**:53–80.
12. Saramito P. Efficient simulation of nonlinear viscoelastic fluid flows. *Journal of Non-Newtonian Fluid Mechanics* 1995; **60**:199–223.
13. Hulsen MA, Fattal R, Kupferman R. Flow of viscoelastic fluids past a cylinder at high Weissenberg number: stabilized simulations using matrix logarithms. *Journal of Non-Newtonian Fluid Mechanics* 2005; **127**:27–39.
14. Coronado OM, Arora D, Behr M, Pasquali M. A simple method for simulating general viscoelastic fluid flows with an alternate log-conformation formulation. *Journal of Non-Newtonian Fluid Mechanics* 2007; **147**:189–199.
15. Pan TW, Hao J. Numerical simulation of a lid-driven cavity viscoelastic flow at high Weissenberg numbers. *Comptes Rendus de l' Academie des Sciences*, *Série I* 2007; **344**:283–286.
16. Chorin AJ, Hughes TJR, Marsden JE, McCracken M. Product formulas and numerical algorithms. *Communications on Pure and Applied Mathematics* 1978; **31**:205–256.
17. Glowinski R. Finite element methods for incompressible viscous flow. In *Handbook of Numerical Analysis*, Ciarlet PG, Lions JL (eds), vol. IX. North-Holland: Amsterdam, 2003; 3–1176.
18. Glowinski R, Pan TW, Hesla T, Joseph DD, Periaux J. A fictitious domain approach to the direct numerical simulation of incompressible viscous flow past moving rigid bodies: application to particulate flow. *Journal of Computational Physics* 2001; **169**:363–426.
19. Pan TW, Glowinski R. Direct simulation of the motion of neutrally buoyant balls in a three-dimensional Poiseuille flow. *Comptes Rendus Mecanique* 2005; **333**:884–895.
20. Lynch DR, Gray WG. A wave equation model for finite element tidal computations. *Computers and Fluids* 1979; **7**:501–534.
21. Wu J. Wave equation models to solve multidimensional transport equations. *International Journal for Numerical Methods in Fluids* 1997; **24**:323–439.
22. Dean EJ, Glowinski R. A wave equation approach to the numerical solution of the Navier–Stokes equations for incompressible viscous flow. *Comptes Rendus de l' Academie des Sciences*, *Série I* 1997; **325**:783–791.
23. Pan TW, Glowinski R. A projection/wave-like equation method for the numerical simulation of incompressible viscous fluid flow modeled by the Navier–Stokes equations. *Journal of Computational Fluid Dynamics* 2000; **9**:28–42.

DOI: 10.1002/fld

24. Wang T, Pan TW, Glowinski R. A comparison of L2-projection and H1-projection methods for the numerical simulation of incompressible viscous fluid flow: a case study. *Chinese Journal of Engineering Mathematics* 2008; **25**.
25. Glowinski R, Guidoboni G, Pan TW. Wall-driven incompressible viscous flow in a two-dimensional semi-circular cavity. *Journal of Computational Physics* 2006; **216**:79–91.
26. Bercovier M, Pironneau O. Error estimates for finite element method solution of the Stokes problem in the primitive variables. *Numerische Mathematik* 1979; **33**:211–224.
27. Bristeau MO, Glowinski R, Periaux J. Numerical methods for the Navier–Stokes equations. Applications to the simulation of compressible and incompressible viscous flow. *Computer Physics Reports* 1987; **6**:73–187.
28. Pakdel P, Spiegelberg SH, McKinley GH. Cavity flows of elastic liquids: two-dimensional flows. *Physics of Fluids* 1997; **9**:3123–3140.
29. Bonito A, Picasso M, Laso M. Numerical simulation of 3D viscoelastic flows with free surfaces. *Journal of Computational Physics* 2006; **215**:691–716.

DOI: 10.1002/fld